Asian Journal of Chemistry; Vol. 27, No. 1 (2015), 297-300

ASIAN JOURNAL OF CHEMISTRY

http://dx.doi.org/10.14233/ajchem.2015.17406

Spectroscopic Study and Green Upconversion of $BaGd_2(MoO_4)_4:Er^{3+}/Yb^{3+}$ Phosphors *via* Cyclic Microwave-Modified Sol-Gel Route

CHANG SUNG LIM

Department of Advanced Materials Science & Engineering, Hanseo University, Seosan 356-706, Republic of Korea

Corresponding author: Tel./Fax: +82 41 6601445; E-mail: cslim@hanseo.ac.kr

Received: 17 February 2014; *Accepted*: 8 May 2014; *Published online*: 26 December 2014; AJC-16559

The double molybdate $BaGd_2(MoO_4)_4:Er^{3+}/Yb^{3+}$ phosphors with the doping concentrations of Er^{3+} and Yb^{3+} (Er^{3+} = 0.05, 0.1, 0.2 and Yb^{3+} = 0.2, 0.45) have been successfully synthesized by a cyclic microwave-modified sol-gel process and the spectroscopic properties have been investigated. The microstructure exhibited well-defined and homogeneous morphology with particles sizes of 1-3 μm. Under excitation at 980 nm, $BaGd_2(MoO_4)_4:Er^{3+}/Yb^{3+}$ particles exhibited a strong 525-nm emission band and a weak 550-nm emission band in the green region and a very weak 655-nm emission band in the red region. The Raman spectra of the particles indicated the presence of strong peaks at higher frequencies and weak peaks at lower frequencies.

Keywords: Upconversion phosphors, Sol-gel, Luminescence, Raman spectroscopy.

INTRODUCTION

Recently, rare-earth-doped upconversion materials have attracted consideration attention because of their unique optical, spectral and chemical properties induced by the special configurations and energy band gaps of the rare earth ions. Rare-earth-doped luminescent materials have been widely applied in the fields, such as lighting sources, display terminals and biological detectors[1-3]. The morphology controlled synthesis of the rare-earth-doped materials are required for well-defined and homogeneous morphology, because their optical properties are dependent on their compositions, crystal structures, shapes and particle sizes[4-6]. Among the rare earth ions, the Er^{3+} ion is suitable for converting infrared to visible light through the upconversion process due to proper electronic energy level configuration. The co-doped Yb^{3+} ion and Er^{3+} ion can remarkably enhance the upconversion efficiency from infrared to visible light due to the efficiency energy transfer from Yb^{3+} to Er^{3+}. The Yb^{3+} ion as a sensitizer can be effectively excited by incident light source energy that is transferred to the activator, from which radiation can be emitted. The Er^{3+} ion activator is the luminescence center of the upconversion particles, while the sensitizer enhances the upconversion luminescence efficiency[7-9].

The rare-earth-doped double molybdates have recently been developed by solid-state reactions[10-14], co-precipitation[15,16], sol-gel method[4-6], hydrothermal method[17,18], Pechini method[19,20], organic gel-thermal decomposition[21] and microwave-assisted hydrothermal method[22]. For practical applications of upconversion phosphors in products, well defined features such as homogeneous particle size distribution and morphology are required. As compared with the usual methods, microwave synthesis has advantages of very short reaction time with the homogeneous morphology features for high purity of final polycrystalline. Microwave heating is delivered to the material surface by radiant and/or convection heating, which is transferred to the bulk of the material *via* conduction[23,24]. A cyclic microwave-modified sol-gel process is a cost-effective method that provides high-quality luminescent materials with easy scale-up in short time periods. However, the cyclic microwave-modified sol-gel process has not been reported.

In this study, $BaGd_2(MoO_4)_4:Er^{3+}/Yb^{3+}$ phosphors with the doping concentrations of Er^{3+} and Yb^{3+} (Er^{3+} = 0.05, 0.1, 0.2 and Yb^{3+} = 0.2, 0.45) were synthesized by the cyclic micro*wave-modified sol-gel process for the first time. The synthesized $BaGd_2(MoO_4)_4:Er^{3+}/Yb^{3+}$ particles were characterized by X-ray diffraction (XRD), scanning electron microscopy (SEM) and energy-dispersive X-ray spectroscopy (EDS). The optical properties were examined comparatively using photoluminescence (PL) emission and Raman spectroscopy.

EXPERIMENTAL

Stoichiometric amounts of $Ba(NO_3)_2$ (99 %, Sigma-Aldrich, USA), $Gd(NO_3)_3·6H_2O$ (99 %, Sigma-Aldrich, USA), $(NH_4)_6Mo_7O_{24}·4H_2O$ (99 %, Alfa Aesar USA), $Er(NO_3)_3·5H_2O$

(99.9 %, Sigma-Aldrich, USA), $Yb(NO_3)_3·5H_2O$ (99.9 %, Sigma-Aldrich, USA), citric acid (99.5 %, Daejung Chemicals, Korea), NH_4OH (A.R.), ethylene glycol (A.R.) and distilled water were used to prepare $BaGd_2(MoO_4)_4$, $BaGd_{1.8}(MoO_4)_4$:$Er_{0.2}$, $BaGd_{1.7}(MoO_4)_4$:$Er_{0.1}Yb_{0.2}$ and $BaGd_{1.5}(MoO_4)_4$:$Er_{0.05}Yb_{0.45}$ compounds. To prepare $BaGd_2(MoO_4)_4$, 0.4 mol % $Ba(NO_3)_2$ and 0.4 mol % $(NH_4)_6Mo_7O_{24}·4H_2O$ were dissolved in 20 mL of ethylene glycol and 80 mL of 5M NH_4OH under vigorous stirring and heating. Subsequently, 0.8 mol % $Gd(NO_3)_3·6H_2O$ and citric acid (with a molar ratio of citric acid to total metal ions of 2:1) were dissolved in 100 mL of distilled water under vigorous stirring and heating. Then, the solutions were mixed together under vigorous stirring and heating. At the end, the highly transparent solutions were obtained and adjusted to pH = 7-8 by the addition of NH_4OH or citric acid. In second way to prepare $BaGd_{1.8}(MoO_4)_4$:$Er_{0.2}$, the mixture of 0.72 mol % $Gd(NO_3)_3·6H_2O$ with 0.08 mol % $Er(NO_3)_3·5H_2O$ was used for formation of the rare earth solution. In third way, to prepare $BaGd_{1.7}(MoO_4)_4$: $Er_{0.1}Yb_{0.2}$, the mixture of 0.68 mol % $Gd(NO_3)_3·6H_2O$ with 0.04 mol % $Er(NO_3)_3·5H_2O$ and 0.08 mol % $Yb(NO_3)_3·5H_2O$ was used for creation of the rare earth solution. In fourth way, to prepare $BaGd_{1.5}(MoO_4)_4$:$Er_{0.05}Yb_{0.45}$, the rare earth containing solution was generated using 0.6 mol % $Gd(NO_3)_3·6H_2O$ with 0.02 mol % $Er(NO_3)_3·5H_2O$ and 0.18 mol % $Yb(NO_3)_3·5H_2O$. The transparent solutions were placed into a microwave oven operating at a frequency of 2.45 GHz with a maximum output-power of 1250 W for 0.5 h. The working cycle of the microwave reaction was controlled precisely between 40 s on and 20 s off for 15 min, followed by further treatment of 30 s on and 30 s off for 15 min. The ethylene glycol was evaporated slowly at its boiling point. The samples were treated with ultrasonic radiation for 10 min to produce a light yellow transparent sol. After this stage, the light yellow transparent sols were dried at 120 °C in a dry oven for 48 h to obtain black dried gels. The black dried gels were grinded and heat-treated at 900 °C for 12 h with 100 °C interval between 600-900 °C. Finally, the white particles were obtained for $BaGd_2(MoO_4)_4$ with pink particles for the doped compositions.

The phase composition of the synthesized particles was identified using XRD (D/MAX 2200, Rigaku, Japan). The microstructure and surface morphology were observed using SEM/EDS (JSM-5600, JEOL, Japan). The PL spectra were recorded using a spectrophotometer (Perkin Elmer LS55, UK) at room temperature. Raman spectroscopy measurements were performed using a LabRam Aramis (Horiba Jobin-Yvon, France). The 514.5 nm line of an Ar ion laser was used as an excitation source and the power on the samples was kept at 0.5 mW.

RESULTS AND DISCUSSION

Fig. 1 shows the XRD patterns of the (a) JCPDS 36-0192 data of $BaGd_2(MoO_4)_4$, the synthesized (b) $BaGd_{1.8}$-$(MoO_4)_4$:$Er_{0.2}$, (c) $BaGd_{1.7}(MoO_4)_4$:$Er_{0.1}Yb_{0.2}$ and (d) $BaGd_{1.5}(MoO_4)_4$:$Er_{0.05}Yb_{0.45}$ particles. All of the XRD peaks could be assigned to the monoclinic-phase $BaGd_2(MoO_4)_4$ with a scheelite-type structure, which was in good agreement with the crystallographic data of $BaGd_2(MoO_4)_4$ (JCPDS 36-1092). This means that the obtained samples have a monoclinic phase with space

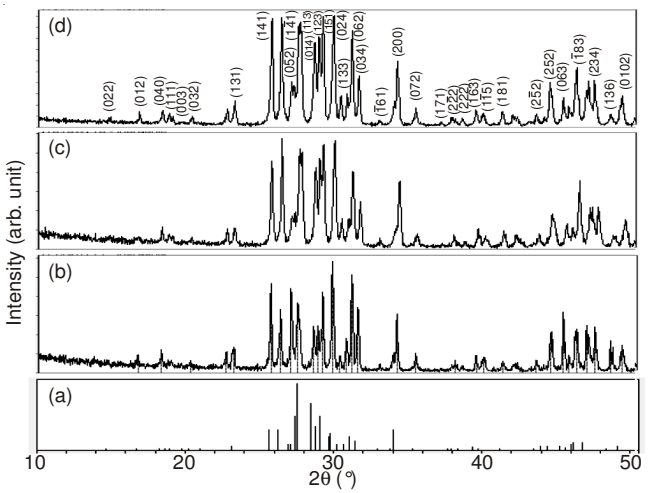

Fig. 1. X-ray diffraction patterns of the (a) JCPDS 36-0192 data of $BaGd_2(MoO_4)_4$, the synthesized (b) $BaGd_{1.8}(MoO_4)_4$:$Er_{0.2}$, (c) $BaGd_{1.7}(MoO_4)_4$:$Er_{0.1}Yb_{0.2}$ and (d) $BaGd_{1.5}(MoO_4)_4$:$Er_{0.05}Yb_{0.45}$ particles

group of C2/c after partially replacing Gd^{3+} by Er^{3+} and Yb^{3+} ions are effectively doped into crystal lattices of the monoclinic $BaGd_2(MoO_4)_4$ phase due to the similar radii of Gd^{3+}, Er^{3+} and Yb^{3+} [4-6]. Post heat-treatment plays an important role in a well-defined crystallized morphology. To achieve a well-defined crystalline morphology, the $BaGd_2(MoO_4)_4$:Er^{3+}/Yb^{3+} phases need to be heat treated at 900 °C for 12 h. It is assumed that the doping amount of Er^{3+}/Yb^{3+} has a great effect on the crystalline cell volume of the $BaGd_2(MoO_4)_4$, because of the different ionic sizes and energy band gap.

Fig. 2 shows SEM images of the synthesized $BaGd_{1.5}(MoO_4)_4$:$Er_{0.05}Yb_{0.45}$ particles. The as-synthesized sample is well crystalline with a fine and homogeneous morphology and particle size of 1-3 μm. The sample has some inhomogeneous particles. It is noted that the doping amounts of Er^{3+} and Yb^{3+} had effects on the morphological features. The combination of doping amounts of 0.02 mol % Er^{3+} and 0.18 mol % Yb^{3+} for $BaGd_{1.5}(MoO_4)_4$:$Er_{0.05}Yb_{0.45}$ has a great effect on the morphological features. Fig. 3 shows the energy-dispersive X-ray spectroscopy patterns of the synthesized (a) $BaGd_{1.8}(MoO_4)_4$:$Er_{0.2}$ and (b) $BaGd_{1.5}(MoO_4)_4$:$Er_{0.05}Yb_{0.45}$ particles and quanti-

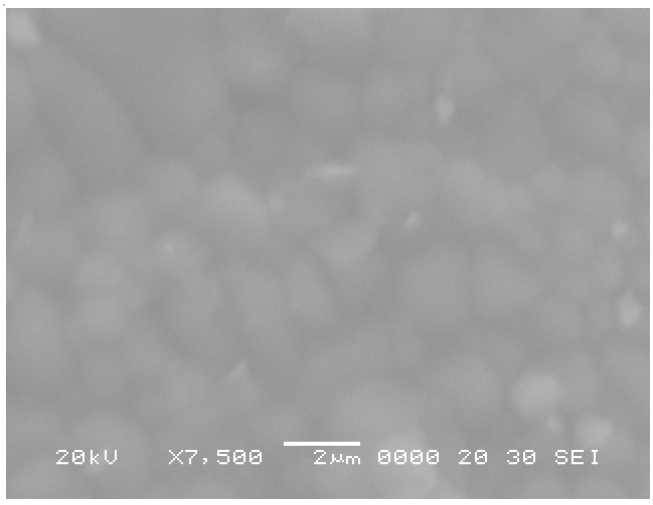

Fig. 2. Scanning electron microscopy images of the synthesized $BaGd_{1.5}(MoO_4)_4$:$Er_{0.05}Yb_{0.45}$ particles

tative results of the synthesized (c) $BaGd_{1.8}(MoO_4)_4:Er_{0.2}$ and (d) $BaGd_{1.5}(MoO_4)_4:Er_{0.05}Yb_{0.45}$ particles. The EDS pattern shows that the (a) $BaGd_{1.8}(MoO_4)_4:Er_{0.2}$ and (b) $BaGd_{1.5}(MoO_4)_4:Er_{0.05}Yb_{0.45}$ particles are composed of Ba, Gd, Mo, O and Er for $BaGd_{1.8}(MoO_4)_4:Er_{0.2}$ and Ba, Gd, Mo, O, Er and Yb for $BaGd_{1.5}(MoO_4)_4:Er_{0.05}Yb_{0.45}$ particles. The quantitative results of (c) and (d) are in good relation with nominal compositions of the particles. The relation of Ba, Gd, Mo, O, Er and Yb components exhibit $BaGd_{1.8}(MoO_4)_4:Er_{0.2}$ and $BaGd_{1.5}(MoO_4)_4:Er_{0.05}Yb_{0.45}$ particles can be successfully synthesized using the cyclic microwave-modified sol-gel process.

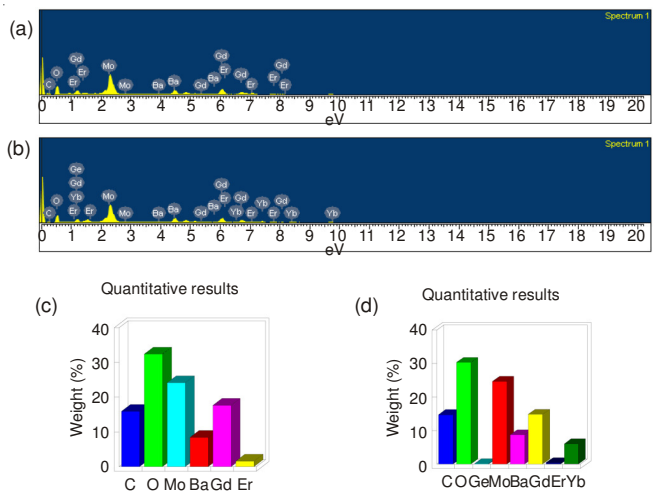

Fig. 3. Energy-dispersive X-ray spectroscopy patterns of the synthesized (a) $BaGd_{1.8}(MoO_4)_4:Er_{0.2}$ and (b) $BaGd_{1.5}(MoO_4)_4:Er_{0.05}Yb_{0.45}$ particles, and quantitative compositions of (c) $BaGd_{1.8}(MoO_4)_4:Er_{0.2}$ and (d) $BaGd_{1.5}(MoO_4)_4:Er_{0.05}Yb_{0.45}$ particles

Fig. 4 shows the upconversion photoluminescence emission spectra of the as-prepared (a) $BaGd_2(MoO_4)_4$, (b) $BaGd_{1.8}(MoO_4)_4$: $Er_{0.2}$, (c) $BaGd_{1.7}(MoO_4)_4:Er_{0.1}Yb_{0.2}$ and (d) $BaGd_{1.5}(MoO_4)_4$:-$Er_{0.05}Yb_{0.45}$ particles excited under 980 nm at room temperature. $BaGd_{1.5}(MoO_4)_4:Er_{0.05}Yb_{0.45}$ particles exhibit a strong 525 nm emission band and a weak 550 nm emission bands in the green region correspond to the $^2H_{11/2} \rightarrow {}^4I_{15/2}$ and $^4S_{3/2} \rightarrow {}^4I_{15/2}$ transitions, respectively, while a weak emission 655 nm band in the red region corresponds to the $^4F_{9/2} \rightarrow {}^4I_{15/2}$ transition. The upconversion intensity of (a) $BaGd_2(MoO_4)_4$ and (b) $BaGd_{1.8}(MoO_4)_4:Er_{0.2}$ have not being detected. The upconversion intensity of (d) $BaGd_{1.5}(MoO_4)_4:Er_{0.05}Yb_{0.45}$ is much higher than that of (c) $BaGd_{1.7}(MoO_4)_4:Er_{0.1}Yb_{0.2}$ particles. Similar results are also observed from Er^{3+}/Yb^{3+} co-doped in other host matrices, which are assigned in the upconversion emission spectra with the green emission intensity ($^2H_{11/2} \rightarrow {}^4I_{15/2}$ and $^4S_{3/2} \rightarrow {}^4I_{15/2}$ transitions) and the red emission intensity ($^4F_{9/2} \rightarrow {}^4I_{15/2}$ transition[5,10,16,25]. The doping amounts of Er^{3+}/Yb^{3+} had a great effect on both the morphological features and their upconversion fluorescence intensity. The Yb^{3+} ion sensitizer can be effectively excited by the energy of the incident light source, which transfers this energy to the activator, where radiation can be emitted. The Er^{3+} ion activator is the luminescence center in upconversion particles and the sensitizer enhances the upconversion luminescence efficiency.

Fig. 5 shows the schematic energy level diagrams of Er^{3+} ions (activator) and Yb^{3+} ions (sensitizer) in the as-prepared

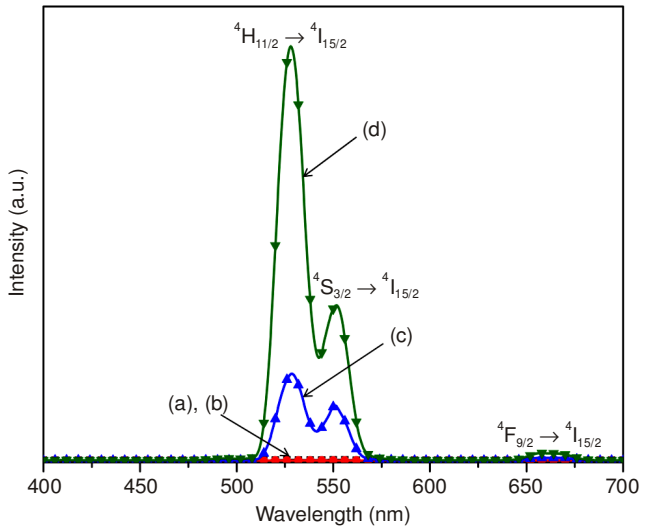

Fig. 4. Upconversion photoluminescence emission spectra of (a) $BaGd_2(MoO_4)_4$, (b) $BaGd_{1.8}(MoO_4)_4:Er_{0.2}$, (c) $BaGd_{1.7}(MoO_4)_4:Er_{0.1}Yb_{0.2}$ and (d) $BaGd_{1.5}(MoO_4)_4:Er_{0.05}Yb_{0.45}$ particles excited under 980 nm at room temperature

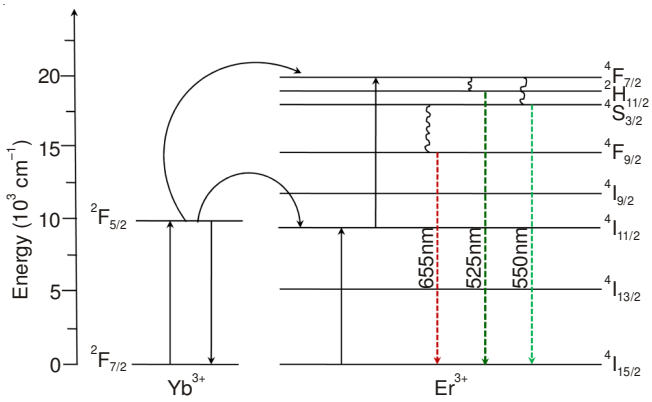

Fig. 5. Schematic energy level diagrams of Er^{3+} ions (activator) and Yb^{3+} ions (sensitizer) in the as-prepared $BaGd_2(MoO_4)_4:Er^{3+}/Yb^{3+}$ system and the upconversion mechanisms accounting for the green and red emissions under 980-nm laser excitation

$BaGd_2(MoO_4)_4:Er^{3+}/Yb^{3+}$ samples and the upconversion mechanisms accounting for the green and red emissions at 980 nm laser excitation. In the complex Er^{3+}/Yb^{3+} co-doped $BaGd_2(MoO_4)_4:Er^{3+}/Yb^{3+}$ ions are initially excited from the ground states to the excited states by the ground state absorption (GSA) processes ($Er^{3+}: {}^4I_{15/2} \rightarrow {}^4I_{11/2}$, $Yb^{3+}: {}^2F_{7/2} \rightarrow {}^2F_{5/2}$) or ET process of $^2F_{5/2}(Yb^{3+}) + {}^4I_{15/2}(Er^{3+}) \rightarrow {}^2F_{7/2}(Yb^{3+}) + {}^4I_{11/2}(Er^{3+})$ dependent on the population of the $^4I_{11/2}$ level in Er^{3+}. It is considered that these three processes are able to populate the $^4F_{7/2}$ level from the $^4I_{11/2}$ level in the Er^{3+} level and then the $^4F_{7/2}$ level relaxes rapidly and non-radiatively to the next lower $^2H_{11/2}$ and $^4S_{3/2}$ in Er^{3+} because of short lifetime of the $^4F_{7/2}$ level. Then, the radiative transitions of $^2H_{11/2} \rightarrow {}^4I_{15/2}$ and $^4S_{3/2} \rightarrow {}^4I_{15/2}$ processes can produce green emissions at 525 and 550 nm[10,26]. For the red emission, the $^4F_{9/2}$ level is populated by non-radiative relaxation from the $^4S_{3/2}$ to the $^4F_{9/2}$ level and cross relaxation (CR) *via* the $^4F_{7/2} + {}^4I_{11/2} \rightarrow {}^4F_{9/2} + {}^4F_{9/2}$ transition in Er^{3+} [35]. Finally, $^4F_{9/2}$ level relaxes radiatively to the ground state at $^4I_{15/2}$ level and releases red emission at 655 nm. The strong 525 and 550 nm emission bands in the green region as shown in Fig. 4 are assigned to the $^2H_{11/2} \rightarrow {}^4I_{15/2}$ and $^4S_{3/2} \rightarrow {}^4I_{15/2}$

transitions of Er^{3+} ions, respectively, while the weak 655-nm emission band in the red region is assigned to $^4F_{9/2} \rightarrow {}^4I_{15/2}$ transition. The higher intensity of the $^4S_{3/2} \rightarrow {}^4I_{15/2}$ transition in comparison with that $^2H_{11/2} \rightarrow {}^4I_{15/2}$ transition may be induced with the concentration quenching effect by the energy transfer between nearest Er^{3+} and Yb^{3+} ions and the interactions between doping ions in $BaGd_2(MoO_4)_4$ host matrix[7,27].

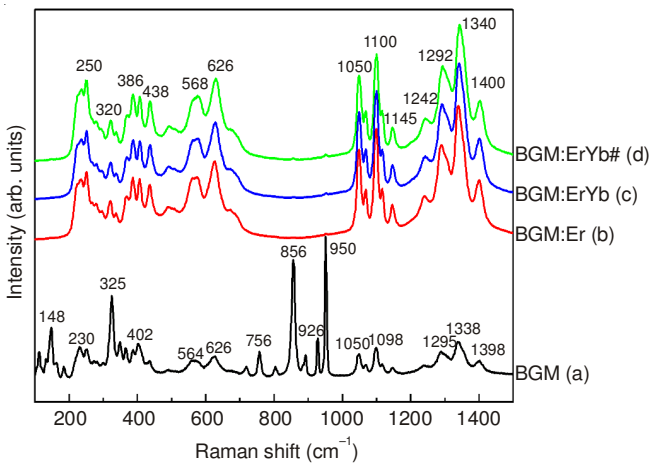

Fig. 6. Raman spectra of the synthesized (a) $BaGd_2(MoO_4)_4$ (BGM), (b) $BaGd_{1.8}(MoO_4)_4:Er_{0.2}$ (BGM:Er), (c) $BaGd_{1.7}(MoO_4)_4:Er_{0.1}Yb_{0.2}$ (BGM:ErYb) and (d) $BaGd_{1.5}(MoO_4)_4:Er_{0.05}Yb_{0.45}$ (BGM:ErYb#) particles excited by the 514.5-nm line of an Ar ion laser at 0.5 mW on the samples

Fig. 6 shows the Raman spectra of the synthesized (a) $BaGd_2(MoO4)_4$ (BGM), (b) $BaGd_{1.8}(MoO_4)_4:Er_{0.2}$ (BGM:Er), (c) $BaGd_{1.7}(MoO_4)_4:Er_{0.1}Yb_{0.2}$ (BGM:ErYb) and (d) $BaGd_{1.5}(MoO_4)_4:Er_{0.05}Yb_{0.45}$ (BGM:ErYb#) particles excited by the 514.5 nm line of an Ar ion laser at 0.5 mW on the samples. The well-resolved sharp peaks for the $BaGd_2(MoO_4)_4$ particles in Fig. 6(a) indicate the high crystallization of the synthesized particles. The internal vibration mode frequencies are dependent on the lattice parameters and the degree of the partially covalent bond between the cation and molecular ionic group $[MoO_4]^{2-}$. The Raman spectra of the (b) $BaGd_{1.8}(MoO_4)_4:Er_{0.2}$ (BGM:Er), (c) $BaGd_{1.7}(MoO_4)_4:Er_{0.1}Yb_{0.2}$ (BGM:ErYb) and (d) $BaGd_{1.5}(MoO_4)_4:Er_{0.05}Yb_{0.45}$ (BGM:ErYb#) particles indicate the domination of strong peaks at higher frequencies (1050, 1100, 1145, 1242, 1292, 1340 and 1400 cm^{-1}) and weak peaks at lower frequencies (250, 320, 386, 438, 568 and 626 cm^{-1}).

Conclusion

The double molybdate $BaGd_2(MoO_4)_4:Er^{3+}/Yb^{3+}$ phosphors with the doping concentrations of Er^{3+} and Yb^{3+} (Er^{3+} = 0.05, 0.1, 0.2 and Yb^{3+} = 0.2, 0.45) were successfully synthesized by a cyclic microwave-modified sol-gel process. Well-crystallized particles were formed after heat treatment at 900 °C for 12 h, showing a fine and homogeneous morphology with particle sizes of 1-3 μm. Under excitation at 980 nm, $BaGd_{1.7}(MoO_4)_4:Er_{0.1}Yb_{0.2}$ and $BaGd_{1.5}(MoO_4)_4:Er_{0.05}Yb_{0.45}$ particles exhibited a strong 525-nm emission band and a weak 550-nm emission band in the green region. The upconversion intensity of the $BaGd_{1.5}(MoO_4)_4:Er_{0.05}Yb_{0.45}$ particles was much higher than that of $BaGd_{1.7}(MoO_4)_4:Er_{0.1}Yb_{0.2}$ particles. The Raman spectra of the $BaGd_{1.8}(MoO_4)_4:Er_{0.2}$, $BaGd_{1.7}(MoO_4)_4:Er_{0.1}Yb_{0.2}$ and $BaGd_{1.5}(MoO_4)_4:Er_{0.05}Yb_{0.45}$ particles indicated the domination of strong peaks at higher frequencies (1050, 1100, 1145, 1242, 1292, 1340 and 1400 cm^{-1}) and weak peaks at lower frequencies (250, 320, 386, 438, 568 and 626 cm^{-1}).

ACKNOWLEDGEMENTS

This study was supported by the Basic Science Research Program through National Research Foundation of Korea (NRF) funded by the Ministry of Science, ICT & Future Planning (2014-046024).

REFERENCES

1. M. Wang, G. Abbineni, A. Clevenger, C. Mao and S. Xu, *Nanomedicine*, **7**, 710 (2011).
2. Y.J. Chen, H.M. Zhu, Y.F. Lin, X.H. Gong, Z.D. Luo and Y.D. Huang, *Opt. Mater.*, **35**, 1442 (2013).
3. C. Zhang, L. Sun, Y. Zhang and C. Yan, *J. Rare Earths*, **28**, 807 (2010).
4. J. Liao, D. Zhou, B. Yang, R. Liu, Q. Zhang and Q. Zhou, *J. Lumin.*, **134**, 533 (2013).
5. J. Sun, Y. Lan, Z. Xia and H. Du, *Opt. Mater.*, **33**, 576 (2011).
6. C. Guo, H.K. Yang and J.H. Jeong, *J. Lumin.*, **130**, 1390 (2010).
7. J. Sun, J. Xian and H. Du, *J. Phys. Chem. Solids*, **72**, 207 (2011).
8. J. Sun, J. Xian, Z. Xia and H. Du, *J. Rare Earths*, **28**, 219 (2010).
9. V.K. Komarala, Y. Wang and M. Xiao, *Chem. Phys. Lett.*, **490**, 189 (2010).
10. H. Du, Y. Lan, Z. Xia and J. Sun, *Mater. Res. Bull.*, **44**, 1660 (2009).
11. L.X. Pang, H. Liu, D. Zhou, G.B. Sun, W.B. Qin and W.G. Liu, *Mater. Lett.*, **72**, 128 (2012).
12. M. Haque and D.K. Kim, *Mater. Lett.*, **63**, 793 (2009).
13. C. Zhao, X. Yin, F. Huang and Y. Hang, *J. Solid State Chem.*, **184**, 3190 (2011).
14. L. Qin, Y. Huang, T. Tsuboi and H.J. Seo, *Mater. Res. Bull.*, **47**, 4498 (2012).
15. Y. Yang, E. Liu, L. Li, Z. Huang, H. Shen and X. Xiang, *J. Alloys Comp.*, **505**, 555 (2010).
16. Y. Tian, B. Chen, B. Tian, R. Hua, J. Sun, L. Cheng, H. Zhong, X. Li, J. Zhang, Y. Zheng, T. Yu, L. Huang and Q. Meng, *J. Alloys Comp.*, **509**, 6096 (2011).
17. Y. Huang, L. Zhou, L. Yang and Z. Tang, *Opt. Mater.*, **33**, 777 (2011).
18. Y. Tian, B. Chen, B. Tian, J. Sun, X. Li, J. Zhang, L. Cheng, H. Zhong, H. Zhong, Q. Meng and R. Hua, *Physica B*, **407**, 2556 (2012).
19. Z. Wang, H. Liang, L. Zhou, J. Wang, M. Gong and Q. Su, *J. Lumin.*, **128**, 147 (2008).
20. Q. Chen, L. Qin, Z. Feng, R. Ge, X. Zhao and H. Xu, *J. Rare Earths*, **29**, 843 (2011).
21. X. Shen, L. Li, F. He, X. Meng and F. Song, *Mater. Chem. Phys.*, **132**, 471 (2012).
22. J. Zhang, X. Wang, X. Zhang, X. Zhao, X. Liu and L. Peng, *Inorg. Chem. Commun.*, **14**, 1723 (2011).
23. C.S. Lim, *Mater. Chem. Phys.*, **131**, 714 (2012).
24. C.S. Lim, *J. Lumin.*, **132**, 1774 (2012).
25. W. Lu, L. Cheng, J. Sun, H. Zhong, X. Li, Y. Tian, J. Wan, Y. Zheng, L. Huang, T. Yu, H. Yu and B. Chen, *Physica B*, **405**, 3284 (2010).
26. J. Sun, J. Xian, X. Zhang and H. Du, *J. Rare Earths*, **29**, 32 (2011).
27. Q. Sun, X. Chen, Z. Liu, F. Wang, Z. Jiang and C. Wang, *J. Alloys Comp.*, **509**, 5336 (2011).